Effects of imperfect premixing coupled with hydrodynamic instability on flame propagation

David Garrido-López, Sutanu Sarkar*

Department of Mechanical and Aerospace Engineering, University of California, San Diego, 9500 Gilman Drive, La Jolla, CA 92093-0411, USA

Abstract

The problem of flame propagation in imperfectly premixed mixtures—mixtures of reactants with variable composition—is considered in this numerical study. We carry out two-dimensional direct numerical simulations of a flame propagating in a globally lean fuel-oxidizer mixture with imposed velocity and composition fluctuations of various intensities. The configuration adopted is that of a flame front interacting with spatially evolving fluctuations, and the characteristic scales of the domain and of the fluctuations imposed are significantly larger than the characteristic thickness of the flame, to account for important flame dynamics such as the hydrodynamic instability. One-step chemistry and Fick's diffusion law are considered, along with unity Lewis number assumption for all the species. It is observed, in agreement with previous results, that relatively weak fluctuations in composition alone may lead to a large increase in flame length and burning rate. The hydrodynamic instability caused by gas expansion, catalyzed by the composition fluctuations interacting with the flame, is found to be responsible for the flame length enhancement. It is observed as well that the relative importance of this effect diminishes as the velocity fluctuations present become more intense, and that composition fluctuations have a small impact on flame length for these cases. It is additionally found that, with increasing intensity of composition fluctuations, there is eventually a reduction of burning rate per unit length of flame which leads, consequently, to a weak reduction of overall burning rate for the largest velocity fluctuation intensities covered by this study.
© 2004 Published by Elsevier Inc. on behalf of The Combustion Institute.

Keywords: Turbulent flames; Inhomogeneous mixtures; Partial premixing; Instability; DNS

1. Introduction

The problem of turbulent flame propagation in imperfectly premixed mixtures has attracted recent interest [1–5] due to its relevance to practical combustion applications, particularly in direct-injection, spark-ignition engines, where the stratified mixture of reactants may contain multi-scale inhomogeneities in composition at the point of ignition. A laboratory study [1] of turbulent propane–air combustion found that, with increasing levels of heterogeneity in the mixture composition, flame wrinkling was enhanced in a monotone fashion, while flame propagation speed increased and then decreased giving an optimal value of heterogeneity. The increase in flame area was especially large for globally lean mixtures, approaching in some cases up to three times the value for the corresponding homogeneous cases.

* Corresponding author. Fax: +1 858 534 7599.
E-mail addresses: dgarrido@mae.ucsd.edu (D. Garrido-López), ssarkar@ucsd.edu (S. Sarkar).

Direct Numerical Simulation (DNS) studies within the configuration of temporally decaying isotropic turbulence for globally lean mixtures [2–4] and globally stoichiometric mixtures [5] agree in observing a reduction in burning rate per unit area of flame caused by the inhomogeneity, and in observing flame area enhancement in the cases of globally lean mixtures. However, the numerical results are not conclusive on the overall impact of these two effects, opposite in sign, on the flame propagation speed. The increase in flame area observed in these numerical studies is, nevertheless, very limited compared with that measured in the experiments of [1].

Although the aforementioned numerical studies have provided valuable insights, they have two major limitations. First, the models employed and the computational capacity available at that time restricted the characteristic scales of the problem and of the velocity and composition fluctuations to values that were small in comparison with practical applications. Second, the temporal decay of the turbulence limited the flame-turbulence interaction to a short period of time. These restrictions might hide important dynamical effects associated with the propagation of the flame. In particular, the hydrodynamic instability related to gas expansion is known to selectively amplify small disturbances along the flame with cutoff and maximum growth rate wavelengths one order of magnitude larger than the characteristic thickness of the flame [6]. As a consequence, flame propagation models, for example [7,8], show that the dynamics of the flame is substantially enriched by the hydrodynamic instability if the dimensions of the flame front are sufficiently large. Recent studies tend to emphasize the impact of the hydrodynamic instability on the wrinkling of turbulent flames as well [9–11].

In this study, we perform DNS of flame propagation in a globally lean fuel-oxidizer mixture, with imposed velocity and composition fluctuations of scales that are much larger than the characteristic thickness of the flame. We employ a computational domain of large dimensions to account for hydrodynamic instability effects, and we adopt the configuration of a flame front interacting with statistically steady fluctuations [12], which allows for long-time simulations of the flame-fluctuation interaction. On the other hand, we restrict the model to two-dimensional flow and make use of a one-step chemical model to make the computational requirements affordable and to cover a wide range of intensity of velocity and composition fluctuations. The objective of the present work was to assess the behavior of the flame under conditions far from extinction; that is, the compositional and velocity fluctuations are not too large. Therefore, a simple chemical model is used with the advantage that a more realistic unsteady flow may be simulated.

2. Governing equations and chemical model

The compressible reacting Navier–Stokes equations are the governing equations in this study. Balance equations of mass, momentum, energy formulated in terms of the pressure, and species mass fractions, along with the equation of state, are employed with the following simplifying assumptions: ideal gas mixture, constant and equal specific heats and molecular masses for all the species, constant viscosity and thermal conductivity, negligible bulk viscosity, and Fick's law for the diffusion terms with the product of the density and the diffusion coefficients assumed to be constant. Soret and Dufour effects, diffusion processes caused by pressure gradients or body forces and heat transfer by radiation, are not considered. Additionally, all the species diffusivities are equal to the thermal diffusivity of the mixture, precluding the existence of any effect of differential diffusion on the results. For all the cases considered here, the ratio of specific heats of the mixture is $\gamma = 1.4$ and the Prandtl number is $Pr = \mu C_P/\kappa = 0.7$, where μ, C_P, and κ stand for the viscosity, specific heat at constant pressure, and thermal conductivity of the mixture, respectively.

Two reactants, namely, fuel F and oxidizer O, one product of combustion P, and an inert species I, are considered. A one-step exothermic irreversible reaction is assumed, $F + (s) O \rightarrow (1 + s) P$, that is, one unit of mass of fuel F reacts with s units of mass of oxidizer O to yield $(1 + s)$ units of mass of product P. The fuel reaction rate is assumed to be $\omega_F = -B\rho^2 Y_F Y_O \exp(-T_{ac}/T)$, where ρ is the density, Y_F and Y_O are fuel and oxidizer mass fractions, respectively, T is the temperature, the frequency parameter B is a constant, and T_{ac} is the activation temperature. In this study, the stoichiometric oxidizer-fuel mass ratio corresponds to propane–air combustion, $s = 3.636$, and oxidizer (oxygen) and inert species are present in fixed proportion in the unburned mixture corresponding to pure air, $r_O = Y_O/(Y_O + Y_I) = 0.232$, where Y_I is the inert mass fraction. The ratio of burned temperature T_b and unburned temperature T_u for the combustion of a stoichiometric mixture is $T_b/T_u = 7.63$, corresponding to a propane–air stoichiometric mixture at 1 atm. and 300 K. The Zeldovich number for stoichiometric composition is $\beta = T_{ac}(T_b - T_u)/T_b^2 = 5.0$. Finally, the frequency parameter B is adjusted so as to obtain a selected low-Mach laminar flame speed, S_L, at stoichiometric conditions.

To capture the experimentally observed variation of S_L with moderate departures from stoichiometric composition, we follow an approach [13] that is different from the traditional approach. The activation temperature is allowed to vary with the mixture fraction variable $Z = (sY_F - Y_O + r_O)/(s + r_O)$ as follows: it is constant for $0.7 < Z/Z_S$

< 1.0 where Z_S is the mixture fraction for the stoichiometric mixture; when $Z > Z_S$, it increases quadratically as $T_{ac} = T_{acS}[1 + C_R(Z/Z_S-1)^2]$; and, when $Z < 0.7Z_S$, it varies as $T_{ac} = T_{acS}[1 + C_L(Z/Z_S-0.7)^2]$. Here, T_{acS} is the selected value of activation temperature for stoichiometric conditions, while C_R and C_L are model parameters set to $C_R = 2$ and $C_L = 3$ so as to match experimental data of propane–air laminar flame speed. Figure 1 presents a comparison of numerical calculations of laminar flame speed as a function of the equivalence ratio $\phi = s Y_F/Y_O$ of the unburned mixture with corresponding experimental data [14,15]. Clearly, the use of variable activation temperature improves the agreement with the experimental data. Note that the local equivalence ratio in the results to be presented in Section 4 is generally in the range $0.6 < \phi < 1.0$, so that the region of validity of this simple model is not violated. Additionally, it has been verified that the increase in activation temperature does not require a refinement in the numerical resolution. This represents an advantage with respect to reduced schemes [16] that are known to add stiffness to the spatial variation of the reaction rate [17].

Finally, to evaluate the gas expansion effect, results are compared with passive reaction simulations, where the heat release is set to zero in the energy equation so that the density does not change due to exothermicity. An additional scalar θ, a virtual temperature that substitutes the real temperature in the reaction rate terms, is calculated with the addition of a balance equation whose source term is $\omega_\theta = -(s/r_O + 1)(T_b - T_u)\omega_F$, the rest of the equation being identical in form to the species mass fraction equations.

3. Numerical method

The governing equations are discretized on a structured mesh. The spatial derivatives are computed using explicit centered fourth-order finite differences generalized for a nonuniform grid. The coefficients involved in the scheme are pre-computed by numerically solving a system of linear equations at each node of the grid as is done in [18] for compact schemes, so that the resultant scheme has strictly fourth-order accuracy. Second-derivative schemes are used for the viscous, conduction, and diffusion terms. All the schemes are biased inward at the nonperiodic boundaries and have locally third-order accuracy. The time-advancement is performed with a low-storage third-order Runge–Kutta scheme [19].

Figure 2 presents a schematic of the problem. A reference laminar flame propagates towards the left in a lean fuel-oxidizer mixture with unburned density ρ_u and temperature T_u. Fluctuations of velocity and composition are imposed at the left boundary and convected into the computational domain to keep the flame brush approximately at a fixed spatial location. After a transient, statistically steady flow is established, with a flame brush region where the reaction occurs in the form of a thin wrinkled premixed flame front. In this study, the reference equivalence ratio of the unburned mixture is $\phi^0 = 0.8$ (reference mixture fraction $Z^0 = 0.0487$), for which the computed reference laminar flame speed is $S_L^0 = 0.68 S_L$. These reference values, along with the characteristic thickness of the reference flame δ_L^0, the unburned density ρ_u, and the unburned temperature T_u, are used for normalization. The reference flame thickness is $\delta_L^0 = (T_b^0 - T_u)/\max(|\nabla T|)$, where $T_b^0 = 6.37 T_u$ is the burned temperature of the reference flame, and $\max(|\nabla T|)$ is the maximum slope of the flame temperature profile.

To keep the flame brush at a fixed spatial location with respect to the inflow boundary, the propagation speed of the flame front is first esti-
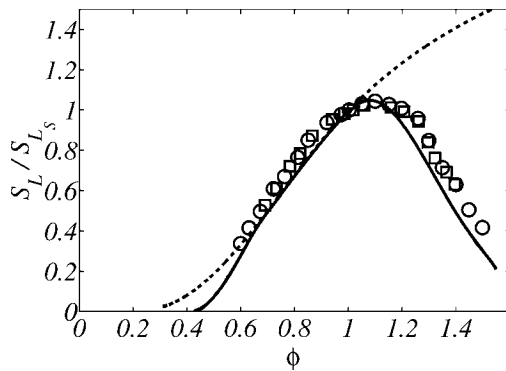

Fig. 1. Variation of laminar flame speed as a function of equivalence ratio for a propane–air mixture at 300 K, 1 atm. Experimental data represented by symbols from [14] (squares) and [15] (circles). Numerical results represented by lines using constant activation temperature (dashed line) and variable activation temperature with mixture fraction (solid line). Each set of data is normalized by its corresponding laminar flame speed at stoichiometric conditions.
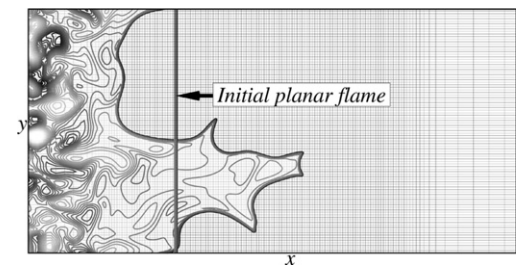

Fig. 2. Computational domain and scheme of the mesh used, along with the initial position of the unperturbed planar flame and a snapshot of fuel mass fraction isocontours of one of the simulations. Mesh size is 2304×1536 points. Domain size is $L_x \times L_y = 340\delta_L^0 \times 167\delta_L^0$, where the flame thickness δ_L^0 is defined in Section 3.

mated using an approximate integral conservation equation for the fuel. At each time step, a Galilean transformation is performed by adding a small change to the longitudinal component of the flow velocity, $u_{new} = u + \Delta u$, with the value of Δu calculated so that the mean inflow velocity becomes equal to the computed front speed. The method has been previously used in the literature [20,21].

Periodic boundary conditions are imposed at the top and bottom sides. The boundary conditions at the left and right sides are implemented in characteristic form [22], generalized to multi-dimensional flow. On the unburned side, the inflow boundary conditions use the data of an inflow domain to impose the temporal change of the incoming characteristic variables: entropy, incoming acoustic coupling of pressure and longitudinal velocity, transverse component of velocity, and species mass fractions. On the burned side, nonreflective boundary conditions are implemented with a pressure correction term as described in [23,24] to keep the mean pressure at the outflow anchored to a specified reference pressure. Since the overall jump of pressure across the flame brush varies depending on the global burning rate, the reference pressure is adjusted in each case to a value that preserves the mean pressure at the inflow.

The computational domain has length $L_x = 340\delta_L^0$ and width $L_y = 167\delta_L^0$, with the initial flame set at a distance of $105\delta_L^0$ from the inflow. The grid spacing, $\Delta_y = 0.107\delta_L^0$, is uniform in the transverse direction. In the central region of length $200\delta_L^0$ encompassing the flame front, the grid spacing is uniform, with $\Delta_x = 0.107\delta_L^0$. The numerical error associated with this grid spacing in the stoichiometric laminar flame speed is found to be less than 10^{-4}. Adjacent to the central region, the grid spacing is smoothly increased, but ensuring that it is significantly smaller than the smallest dynamic scale, estimated using the enstrophy dissipation scale $\eta_d = (v/\omega_z')^{0.5}$ [25], where ω_z' is the root mean square (rms) of the vorticity fluctuations.

The inflow fields are the result of separate simulations of temporally decaying isotropic turbulence. The velocity and composition fluctuations are initialized with approximate energy and scalar spectra [25], both having peaks at the same lengthscale, and with random phase modes. The simulations are run sufficiently long to allow the velocity and composition fluctuations to acquire the correct spectra and phase relationships.

The intensity of the velocity fluctuations interacting with the flame front is estimated by averaging the values of velocity along the periodic direction and along time at a longitudinal station at the beginning of the flame brush. The characteristic lengthscales of the velocity fluctuations are calculated at this station as well. The mean Z_f and the rms Z_f' of the mixture fraction fluctua-

tions at the flame front are estimated using the interpolated values of mixture fraction at the isotherm, $T_1 = 2T_u$, located well inside the preheat zone. The length of the premixed flame front L_f is estimated by numerically calculating the length of the same isothermal line. Finally, the overall fuel burning rate $\dot{m}_F$ is obtained by integration of the fuel reaction rate ω_F over the computational domain.

In the simulations, a relatively long time, $t_i = O(L_y/S_L^0)$, is required until the front reaches a statistically steady state, albeit very chaotic and intermittent. The time span of the simulations after the transient, used to sample the statistics, is approximately 200–$250\delta_L^0/S_L^0$ using about 80–100 flow fields for all the cases. Each simulation, with a domain of 2304×1536 points, required about 5000 CPU hours running on either 64 or 128 IBM Power3 processors.

4. Results and discussion

Table 1 presents the normalized values of the rms of the velocity fluctuations u', enstrophy dissipation scale η_d, Taylor microscale $\lambda = u'/(\partial u/\partial x)'$, microscale Reynolds number $Re_\lambda = (\rho_u u'\lambda)/\mu$, and time-averaged rms of mixture fraction fluctuations at the flame front Z_f', for all the cases. In summary, four different intensities of velocity fluctuations from zero to approximately three times the reference flame speed have been imposed at the inflow. For each choice of u', cases with different values of Z_f' have been run. The characteristic scales of the composition fluctuations imposed in series A are similar to those of series B.

Figure 3 shows the time average of the fuel burning rate, $\langle \dot{m}_F \rangle$, normalized by that corresponding to the reference flame, $\dot{m}_F^0$. There is a large increase in burning rate caused by the com-

Table 1
Parameters of the different cases simulated

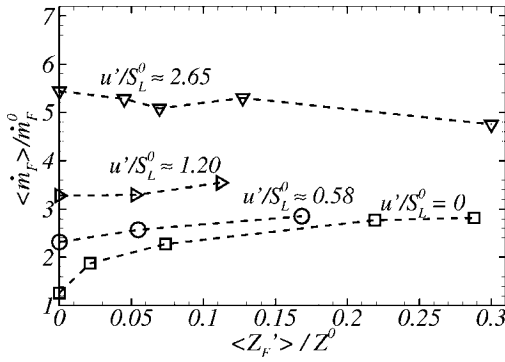| Run	$\frac{u'}{S_L^0}$	$\frac{Z_f'}{Z^0}$	$\frac{\eta_d}{\delta_L^0}$	$\frac{\lambda}{\delta_L^0}$	Re_λ
A0	0.00	0.000	—	—	—
A1	0.00	0.021	—	—	—
A2	0.00	0.074	—	—	—
A3	0.00	0.212	—	—	—
A4	0.00	0.288	—	—	—
B0	0.54	0.000	1.8	10.5	16
B1	0.58	0.055	1.8	10.7	18
B2	0.60	0.168	1.8	10.6	18
C0	1.18	0.000	1.2	8.9	30
C1	1.19	0.053	1.2	9.5	32
C2	1.26	0.112	1.2	9.0	32
D0	2.60	0.000	0.8	7.6	56
D1	2.55	0.045	0.8	8.0	58
D2	2.65	0.069	0.8	7.5	57
D3	2.67	0.127	0.8	7.4	56
D4	2.67	0.300	0.8	7.4	56

See text for explanation.

Fig. 3. Variation of average burning rate as a function of intensity of mixture fraction fluctuations for different levels of u'/S_L^0. Cases A0–A4 are represented by squares, cases B0–B2 by circles, cases C0–C2 by triangles, and cases D0–D4 by inverted delta symbols.

position fluctuations in series A, where no velocity fluctuations are present, and it eventually levels off for $Z_f'/Z^0 > 20\%$ to a value close to three times the reference burning rate. These results are consistent with the findings of [1]. The figure also shows burning rate enhancement in series B with small $u'/S_L^0 \approx 0.58$. The effect of the composition fluctuations is more moderate in series C with higher $u'/S_L^0 \approx 1.20$. In series D with highest $u'/S_L^0 \approx 2.65$, there is a *qualitative* change; increasing levels of inhomogeneity in the mixture composition lead to a reduction of the overall burning rate.

Figure 4A presents the time-averaged flame length, $\langle L_f \rangle$, normalized by the planar flame length, L_f^0. Increasing levels of inhomogeneity lead to the generation of flame wrinkling and augmentation of flame length, explaining the burning rate enhancement noted above, and there is a general increase for all levels of u'/S_L^0. Figure 4B, where the flame length is normalized by the average flame length of the corresponding case with $Z' = 0$, shows a different picture, however; the *relative* effect of inhomogeneities on the flame length is weaker as u'/S_L^0 increases. The reasons for the strong impact observed on the flame length in series A and B and the weakening of this impact in series C and D are discussed later.

Figure 5 shows the time average of the burning rate per unit flame length, $\langle \dot{m}_F/L_f \rangle$, normalized by the value of the corresponding case with $Z_f' = 0$. The figure shows that there is a monotone reduction in burning rate per unit length of flame with increasing levels of composition fluctuations. This effect was already pointed out in [2–5]. The cause of this reduction is a shift in the mean mixture fraction at the flame front toward leaner values due to the increased residence time of the flame in zones where the mixture is leaner than the average [2]. Here, the data suggest that this effect is
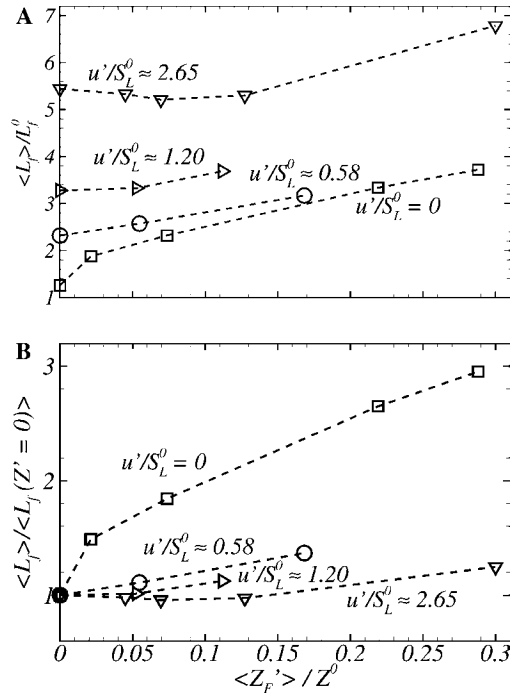

Fig. 4. Variation of average flame length as a function of intensity of mixture fraction fluctuations. (A) Values normalized by the length of the planar flame. (B) Values of each group normalized by the average flame length of the corresponding case with $Z_f' = 0$. Lines and symbols as in Fig. 3.
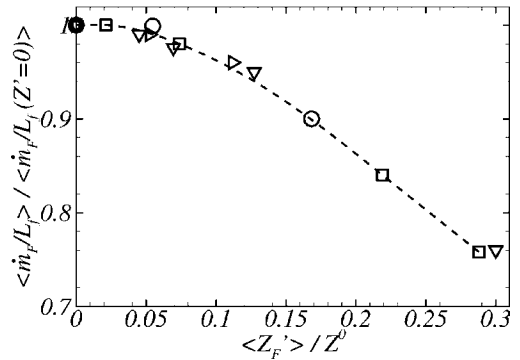

Fig. 5. Time average of the burning rate per unit flame length. The dashed curve is an estimated fit to show the general trend. Symbols as in Fig. 3.

independent of the intensity of the velocity fluctuations present, since all the data fall approximately on the same curve. The one-step chemical model and the unity Lewis number assumption adopted lead to a flat response of the local burning rate to flame stretch [26], explaining the collapse of the data. However, the degree of

collapse in a model with more realistic thermochemistry needs to be ascertained. Figs. 4B and 5 combined explain why, for small u'/S_L^0, the overall burning rate increases with increasing compositional fluctuations, opposite to the trend at large u'/S_L^0 of decreasing burning rate with increasing compositional fluctuations. In the first case, the large increase of flame length, Fig. 4B, dominates over the reduction in burning rate per unit length, Fig. 5, while the augmented flame length loses relative importance when the velocity fluctuations present are more intense and is not sufficient to overcome the reduction in burning rate per unit length.

To evaluate the impact of gas expansion on the results, simulations were run using the passive reaction formulation excluding variation of density caused by exothermicity. The initial setup and the fluctuations imposed at the inflow boundary are identical to the active reaction cases with which a direct comparison is sought. Figure 6 compares the time evolution of the burning rate for case A2, where only fluctuations in composi-
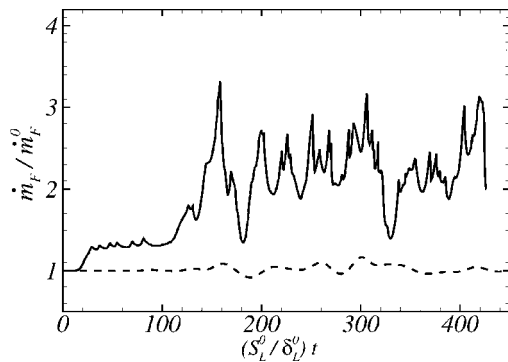

Fig. 6. Time evolution of burning rate for case A2 (solid line) and the corresponding passive reaction case (dashed line).
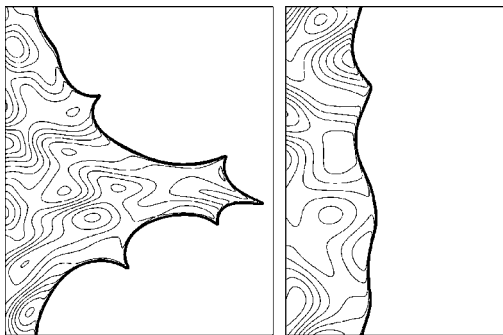

Fig. 7. Snapshot of fuel mass fraction isocontours for case A2 (left) and the corresponding passive reaction case (right).

tion of small intensity are present, with the corresponding passive reaction case. The burning rate in the former is very unsteady, having large spiky departures from the average value of 2.28 times the burning rate of the planar flame, while in the latter case, the inhomogeneity has negligible effect on the burning rate. Figure 7 compares a snapshot of the fuel mass fraction isocontours in both simulations. Direct observation of the flame front evolution in case A2 reveals that the front has a cellular pattern perturbed by the composition fluctuations, with the formation of deep tongues toward the burned side, in contrast to the weak distortion of the front in the passive reaction case. This implies that the wrinkling of the flame has a significant contribution from the destabilizing effect of gas expansion. Interestingly, it is observed that the effect of small-intensity velocity fluctuations on the burning rate in case B0 is very similar to that of small-intensity composition fluctuations in case A2, with an average value of 2.32 times the reference burning rate, while the corresponding passive reaction case shows an average burning rate well under this value. These observations suggest that relatively weak fluctuations of both velocity and composition fluctuations are able to *catalyze* the instability of the front, giving a physical explanation for the strong increase in flame length and burning rate observed in cases A1–A4 and B0–B2.

As illustrated in Fig. 7, it is observed that the flame front in series A and B develops deep wrinkles of scales that are of the order of the transverse size of the domain, consistent with the evolution of flame fronts subject to the Darrieus–Landau instability [7,8]. The extent of this large-scale wrinkling is evaluated for all the cases as follows. The density field at a particular time is filtered in the x-direction with a top-hat filter. The objective of this operation is to reduce the isochoric line $\rho_1 = 0.5\rho_u$ of the filtered density field to a single-valued function of the transverse coordinate, $x_{\rho 1} = f(y)$. To achieve this, the stencil of the filter must have large dimensions, $\Delta_f = 0.9L_y$. It has been verified that further increase in the size of the filter does not affect the shape of $f(y)$. The function, $f(y)$, is then Fourier decomposed, and only the first two modes with wavelengths L_y and $L_y/2$ are retained. The resulting filtered flame shape isolates the large-scale distortion of the flame front devoid of fluctuation-scale wrinkling. Figure 8 shows a comparison of the flame front with the filtered flame shape for a particular time in case D2.

Figure 9 shows the normalized average length of the filtered flame shape, $\langle \bar{L}_f \rangle / L_f^0$. The presence of a weak level of fluctuations in cases A1, A2, B0, and B1 leads to values of $\langle \bar{L}_f \rangle / L_f^0$ of around 1.5, representing a significant contribution to the total flame length for those cases, see Fig. 4A. However, $\langle \bar{L}_f \rangle / L_f^0$ saturates to around that value
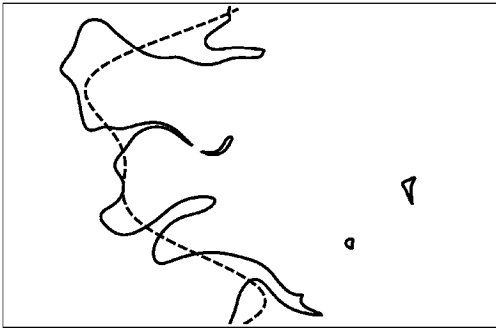
Fig. 8. Snapshot of isocontour $T = 2T_u$ for case D2 and the corresponding filtered flame shape.
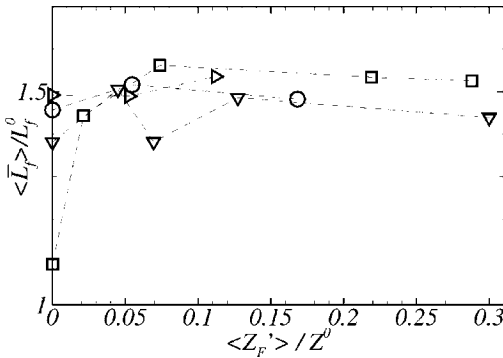

Fig. 9. Average length of the filtered flame shape. Lines and symbols as in Fig. 3.

for the rest of the cases, indicating that, as the fluctuations become more intense, the flame length is increased mainly by fluctuation-scale wrinkling, multiplied by a constant factor of around 1.5 brought about by the large-scale distortion. The fact that, after a certain fluctuation level, the large-scale distortion is not enhanced with increasing fluctuation intensity explains in part why the addition of composition fluctuations has a weaker effect on the flame length in series C and D relative to series A. Moreover, passive reaction simulations, where the large-scale distortion of the front is minimal in the absence of thermal expansion, reveal that the fluctuation-scale wrinkling caused by composition fluctuations of any intensity in the range covered is relatively small compared to that generated by the velocity fluctuations of intensity $u'/S_L^0 \approx 2.65$ (for a case with $Z_f'/Z^0 = 28\%$ and $u'/S_L^0 = 0$, the average length obtained is $1.6L_f^0$, while for a case with $u'/S_L^0 = 2.6$ and $Z_f'/Z^0 = 0$, the average length obtained is $3.6L_f^0$).

These results stress the importance of accounting for the effect of the hydrodynamic instability in the problem of flame propagation when the scale of the problem and that of the fluctuations present are both much larger than the flame thick-

ness. Finally, there is confidence in the reproducibility of these results in three-dimensional simulations, encouraged by their consistency with experiments [1] and by evidence in the literature [27,28], indicating that the hydrodynamic instability enhances the flame wrinkling in three-dimensional flows as much as it does in two-dimensional models.

5. Conclusions

The propagation of a lean fuel-oxidizer flame in an imperfectly premixed mixture has been studied via two-dimensional simulations at larger scale and longer time than previously accessed by DNS. The conclusions of this work are as follows.

Increasing levels of inhomogeneity in mixture composition lead to a significant enhancement of the flame length when the velocity fluctuations present are of small intensity ($u'/S_L < 1$), and to a weak enhancement of the flame length when the velocity fluctuations present are more intense.

Increasing levels of inhomogeneity lead to a reduction of burning rate per unit length of flame, related to a shift in the average mixture fraction at the flame toward leaner values, and this effect seems, under the assumed thermochemistry, independent of the intensity of the velocity fluctuations present.

Increasing the rms mixture fraction fluctuation can cause either increase of the overall burning rate if the velocity fluctuations present are relatively weak ($u'/S_L < 1$), or decrease in the burning rate if the velocity fluctuations present are more intense. In the former, the effect of flame length generation dominates over the reduction in burning rate per unit length of flame, while the opposite happens in the latter.

By comparison with passive reaction simulations, a large-scale distortion originating from the hydrodynamic instability is clearly identified. It is found that both velocity and composition fluctuations of small intensity are able to catalyze this large-scale distortion, with the consequent flame length increase. This effect explains the significant impact of composition fluctuations on flame length when velocity fluctuations present are of small intensity.

The large-scale distortion of the front saturates to an approximately constant value when fluctuation intensities increase. Further flame length increase is mainly promoted by fluctuation-scale wrinkling. Moreover, it is found that the local wrinkling induced by the composition fluctuations is small compared to that generated by the velocity fluctuations for the range of intensities covered here. These findings taken together explain the reduced impact of composition fluctuations on flame length when velocity fluctuations present are more intense.

Finally, it is worth recalling the unity Lewis number assumption made in this study. Although the conclusions are not expected to qualitatively change, future simulations to assess the additional effect of nonunity Lewis number and preferential diffusion effects would be helpful.

Acknowledgments

Appendix A. Supplementary data

Supplementary data associated with this article can be found in the online version at doi:10.1016/ j.proci.2004.07.014.

References

[1] J. Zhou, K. Nishida, T. Yoshizaki, H. Hiroyasu, *SAE paper* 982563 (1998).
[2] T. Poinsot, D. Veynante, A. Trouvé, G. Ruesch, in: *Proceedings of the Summer Program 1996*, Center for Turbulence Research, NASA Ames/Stanford University, 1996, pp. 111–141.
[3] D.C. Haworth, R.J. Blint, B. Cuenot, T.J. Poinsot, *Combust. Flame* 121 (2000) 395–417.
[4] C. Jiménez, B. Cuenot, T. Poinsot, D. Haworth, *Combust. Flame* 128 (2002) 1–21.
[5] J. Hélie, A. Trouvé, *Proc. Combust. Inst.* 27 (1998) 891–898.
[6] P. Pelce, P. Clavin, *J. Fluid Mech.* 124 (1982) 219–237.
[7] G. Joulin, P. Cambray, *Combust. Sci. Technol.* 81 (1992) 243–256.
[8] W.T. Ashurst, *Combust. Theory Modelling* 1 (1997) 405–428.
[9] H. Boughanem, A. Trouvé, *Proc. Combust. Inst.* 27 (1998) 971–978.
[10] H. Kobayashi, H. Kawazoe, *Proc. Combust. Inst.* 28 (2000) 375–382.
[11] K.L. Pan, J. Qian, C.K. Law, W. Shyy, *Proc. Combust. Inst.* 29 (2002) 1695–1704.
[12] S. Zhang, C.J. Rutland, *Combust. Flame* 102 (1995) 447–461.
[13] F.A. Williams, personal communication, 2002.
[14] D.L. Zhu, F.N. Egolfopoulos, C.K. Law, *Proc. Combust. Inst.* 22 (1988) 1537–1545.
[15] C.M. Vagelopoulos, F.N. Egolfopoulos, *Proc. Combust. Inst.* 27 (1998) 513–519.
[16] C. Westbrook, F. Dryer, *Combust. Sci. Technol.* 27 (1981) 31–43.
[17] T. Poinsot, D. Veynante, *Theoretical and Numerical Combustion.* Edwards, Philadelphia, PA, 2001, p. 54.
[18] L. Gamet, F. Ducros, F. Nicoud, T. Poinsot, *Int. J. Numer. Methods Fluids* 29 (1999) 159–191.
[19] J.H. Williamson, *J. Comput. Phys.* 35 (1980) 48–56.
[20] B. Denet, P. Haldenwang, *Combust. Sci. Technol.* 104 (1995) 143–167.
[21] L. Vervisch-Guichard, J. Reveillon, R. Hauguel, in: *Turbulence and Shear Flow Phenomena, Second International Symposium*, KTH, Stockholm, 2001, pp. 513–518.
[22] K.W. Thompson, *J. Comput. Phys.* 89 (1990) 439–461.
[23] D.H. Rudy, J.C. Strikwerda, *J. Comput. Phys.* 36 (1980) 55–70.
[24] T.J. Poinsot, S.K. Lele, *J. Comput. Phys.* 101 (1992) 104–129.
[25] M. Lesieur, *in: Turbulence in Fluids*, third ed. Kluwer academic publishers, Dordrecht, The Netherlands, 1997, pp. 285–313.
[26] F.A. Williams, *Combustion theory*, second ed. Addison Wesley, Redwood City, CA, 1985, p. 421.
[27] S. Kadowaki, *Phys. Fluids* 11 (1999) 3426–3433.
[28] V.V. Bychkov, M.A. Liberman, *Phys. Rep.* 325 (2000) 115–237.

Comment

Ravi Sangras, American Air Liquide, USA. Could you comment on why the concentration fluctuations increase flame speed when $u'/S_L < 1$ but have no effect when $u'/S_L > 1$?

Reply. The explanation in the paper and in the presentation is summarized below. Composition fluctuations in an overall lean mixture with zero velocity fluctuations increase the flame speed because, first, there is a direct effect associated with the leading head of the flame front lying preferentially in richer regions with higher-than-average laminar flame speed and, second, there is an indirect effect of flame area increase owing to large-scale front distortion originating from the hydrodynamic instability. The direct effect is roughly order ΔS_L, the range of laminar flame speed in the inhomogeneous mixture. For $u'/S_L > 1$, the direct effect of order ΔS_L is no longer significant relative to the increase in flame speed, order u', brought about by the velocity fluctuations. Furthermore, the area increase brought about by the hydrodynamic instability saturates at $u'/S_L \approx 1$, see Fig. 9.